On the manipulation of flow and acoustic fields of a blunt trailing edge aerofoil by serrated leading edges

Seyed Mohammad Hasheminejad, Tze Pei Chong, Giovanni Lacagnina, Phillip Joseph, Jung-Hoon Kim, Kwing-So Choi, Mohammad Omidyeganeh, Alfredo Pinelli, and Oksana Stalnov

Citation: The Journal of the Acoustical Society of America **147**, 3932 (2020); doi: 10.1121/10.0001377
View online: https://doi.org/10.1121/10.0001377
View Table of Contents: https://asa.scitation.org/toc/jas/147/6
Published by the Acoustical Society of America

JASA ARTICLE

On the manipulation of flow and acoustic fields of a blunt trailing edge aerofoil by serrated leading edges

Seyed Mohammad Hasheminejad,[1,a)] Tze Pei Chong,[1,b)] Giovanni Lacagnina,[2,c)] Phillip Joseph,[2,d)] Jung-Hoon Kim,[3] Kwing-So Choi,[3,e)] Mohammad Omidyeganeh,[4] Alfredo Pinelli,[4,f)] and Oksana Stalnov[5,g)]

[1]*Department of Mechanical and Aerospace Engineering, Brunel University London, Uxbridge, UB8 3PH, United Kingdom*

[2]*Institute of Sound and Vibration Research, University of Southampton, Southampton, SO17 1BJ, United Kingdom*

[3]*Fluids and Thermal Engineering Group, University of Nottingham, Nottingham, NG7 2RD, United Kingdom*

[4]*School of Mathematics, Computer Science and Engineering, City University London, London, EC1V 0HB, United Kingdom*

[5]*Faculty of Aerospace Engineering, Technion Israel Institute of Technology, Israel*

ABSTRACT:

This paper employs serrated leading edges to inject streamwise vorticity to the downstream boundary layer and wake to manipulate the flow field and noise sources near the blunt trailing edge of an asymmetric aerofoil. The use of a large serration amplitude is found to be effective to suppress the first noise source—bluntness-induced vortex shedding tonal noise—through the destruction of the coherent eigenmodes in the wake. The second noise source is the instability noise, which is produced by the interaction between the boundary layer instability and separation bubble near the blunt edge. The main criterion needed to suppress this noise source is related to a small serration wavelength because, through the generation of more streamwise vortices, it would facilitate a greater level of destructive interaction with the separation bubble. If the leading edge has both a large serration amplitude and wavelength, the interaction between the counter-rotating vortices themselves would trigger a turbulent shear layer through an inviscid mechanism. The turbulent shear layer will produce strong hydrodynamic pressure fluctuations to the trailing edge, which then scatter into broadband noise and transform into a trailing edge noise mechanism. This would become the third noise source that can be identified in several serrated leading edge configurations. Overall, a leading edge with a large serration amplitude and small serration wavelength appears to be the optimum choice to suppress the first and second noise sources and, at the same time, avoid the generation of the third noise source.

 https://doi.org/10.1121/10.0001377

(Received 2 February 2020; revised 4 May 2020; accepted 15 May 2020; published online 16 June 2020)

[Editor: Alan Thomas Wall] Pages: 3932–3947

I. INTRODUCTION

Self-noise radiated from an aerofoil trailing edge has always been a concern in many industrial applications such as turbomachinery, fans, and propellers. A prerequisite to produce low-noise lifting surfaces is to understand the trailing edge noise sources and their generating mechanisms, and as many as five types have been identified by Brooks *et al.* (1989). One of these is produced by the separation of free shear layers from sharp corners of a blunt trailing edge. If the blunt thickness is more than 30% larger than the boundary layer displacement thickness across a relatively large range of the Reynolds number, the wake is expected to exhibit the characteristic of vortex shedding (Blake, 1986; Brooks and Schlinker, 1983). Although trailing edge bluntness can have aerodynamic and structural advantages in some cases (Standish and Van Dam, 2003; Winnemöller and Dam, 2007), the unsteady wake vortex shedding can also increase in drag, induce structural dynamic instability, and emit large amplitude narrowband tonal noise into the far field. When a large bluntness on an engineering body is unavoidable due to the manufacturing constraint, mitigations, such as the application of either active or passive flow control, may be required in order to disrupt the formation of vortex shedding behind the body and reduce the radiated aerodynamic noise.

So far, almost all the control strategies are exclusively applied at the vicinity of the trailing edge. For example, attaching a splitter plate behind a bluff body can extend the separating shear layers to further downstream, thereby preventing/delaying the entrainment of the outer flow to the base region to starve off the tendency of vortex shedding (Roshko, 1995). Another passive control strategy is to replace the blunt edge with a porous surface and facilitate cross-flow between the top and bottom surfaces to reduce the difference in base pressure near the blunt face

[a)]ORCID:0000-0002-7717-0820.
[b)]Electronic mail: t.p.chong@brunel.ac.uk, ORCID:0000-0002-5272-3943.
[c)]ORCID:0000-0002-8038-1127.
[d)]ORCID:0000-0001-9299-8629.
[e)]ORCID:0000-0002-8383-8057.
[f)]ORCID:0000-0001-5564-9032.
[g)]ORCID:0000-0002-3853-1507.

https://doi.org/10.1121/10.0001377

(Showkat Ali *et al.*, 2018). Recently, Al-Sadawi *et al.* (2019) showed that the dielectric barrier discharge (DBD) plasma actuator can be used to reduce the bluntness-induced vortex shedding noise. The basis of their control approach is to attach the DBD plasma actuators at the vicinity of the blunt trailing edge to generate ionised secondary flow. In one particular plasma configuration, Al-Sadawi *et al.* (2019) show that the body force of the ionised air can be manipulated such that disruptive flow structures with a strong streamwise vorticity are injected into the otherwise dominant spanwise vorticity field produced by the wake vortex shedding. To a certain extent, the mechanism is not too different from the control of flow separation by the vortex generator on an aircraft wing (Lin, 2002).

Undulating the frontal part of an aerofoil could introduce local acceleration and deceleration forcing, alternatively, across the span. This would trigger a shear instability that transforms into vortical structures with a significant streamwise vorticity level in a manner similar to that generated by the array of vortex generators. The so-called leading edge serration is well known for its capability to improve the aerodynamic performance of aerofoil at the post-stall regime by generating streamwise vortices to transfer high momentum flow from the free stream to the boundary layer (Miklosovic *et al.*, 2004; Johari *et al.*, 2007; Hansen *et al.*, 2011; Rostamzadeh *et al.*, 2012). This process results in a shrinking or an outright suppression of the separation zone near the leading edge, thus, minimising the tendency for stall (Van Nierop *et al.*, 2008; Fish *et al.*, 2011; Skillen *et al.*, 2015).

Besides the improvement in aerodynamic performance, leading edge serration is also studied extensively for the reduction of turbulence–aerofoil interaction noise (Kim *et al.*, 2016; Biedermann *et al.*, 2017; Chaitanya *et al.*, 2017). It was reported that the mechanisms of leading edge noise reduction by serration are related to the de-correlation of the surface pressure fluctuation and the far field noise on the serrated leading edge, as well as the acoustical phase interference and destruction effect between the serration peak and the mid-region of the oblique edge. Thus, leading edge noise reduction by serration only happens *in situ*. In other words, the generated vortical structures by the serration cannot directly influence the leading edge noise radiation. Chong *et al.* (2018) show that leading edge serrations with a sufficiently large serration amplitude can form large-scale vortical structures within the boundary layer that can overcome the viscous dissipation and continue to develop until the trailing edge. When mixed with the arriving vortical structures, they observe an enhanced three-dimensionality of the turbulent boundary layer near the trailing edge as well as a disintegration of the large-scale fluctuations. This leads to their hypothesis that a serrated leading edge can manipulate the trailing edge noise source and affect the acoustical scattering efficiency locally.

As will be shown later, the vortical structures generated from a serrated leading edge not only can reach the trailing edge relatively intact, but also can sustain well into the wake. To the authors' best knowledge, no work has been presented to date that considers the effect of leading edge serrations on the vortex shedding tonal noise induced by a blunt trailing edge. This paper aims to shed new light on whether the leading edge serrations can be an effective control device to manipulate the vortex shedding and change the radiated tonal noise characteristics. For this purpose, far field noise and wake flow measurements were undertaken for a NACA 65(12)-10 aerofoil with a blunt trailing edge and subjected to four different serrated leading edge geometries.

II. EXPERIMENT SETUP AND MEASUREMENT TECHNIQUES

The aerofoil section investigated in the current study is the NACA 65(12)-10. In its original profile, i.e., with a sharp trailing edge, it has a chord length of $C = 0.15$ m. The overall span length of the aerofoil is 0.5 m, but only 0.3 m is submerged into the open jet flow to fit the nozzle width, while the remaining part would protrude from the side holding plates. As shown in Fig. 1, the aerofoil model consists of a main body, a detachable frontal part that allows changeover of different leading edge profiles, and a truncated trailing edge at $s/C = 0.87$, resulting in a blunt thickness of $d = 5$ mm. This will achieve a typical bluntness to the boundary layer displacement thickness ratio of 1.4, significantly larger than the minimum value of 0.3 needed for vortex shedding to occur (Blake, 1986). Note that s and x are defined as the streamwise distances measured from the aerofoil leading edge (straight) and blunt trailing edge, respectively. In addition to the straight leading edge that serves as the baseline, four different types of serrated leading edges were investigated in this study. All the serrated leading edges exhibit a sinusoidal pattern, which is defined by two geometrical parameters: serration wavelength (L) and serration amplitude (H). These parameters are then used in the description of the test model notations. For example, the model "$H45L7.5$" refers to the serrated leading edge geometry with $H = 45$ mm and $L = 7.5$ mm. The results will often be compared to the "baseline" configuration, which represents the aerofoil with a straight leading edge. The serration geometries are illustrated in Fig. 1, which also includes a table to summarise all of the combinations of H and L for the serrated leading edges investigated in this study. A design principle adopted here is to maintain the same wetted area between the baseline and serrated aerofoils. To achieve this, the leading edge serration has to include both the "cut-in" and "add-on" features, i.e., $H/2$ of the serration protrudes from the otherwise baseline straight leading edge, and the remaining $H/2$ would be a cut-in.

Both the far field and flow measurements were performed in the aeroacoustics wind tunnel at Brunel University London (UK). The open jet type wind tunnel, which has a rectangular nozzle exit of 0.10 m (height) $\times$ 0.30 m (width), is situated inside a 4 m $\times$ 5 m $\times$ 3.4 m anechoic chamber. The wind tunnel is designed so that the background noise of the facility is sufficiently below the

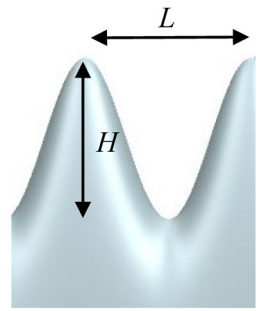

	H (serration amplitude)	L (serration wavelength)
Baseline	0	0
*H*7.5*L*7.5	7.5	7.5
*H*7.5*L*45	7.5	45
*H*45*L*7.5	45	7.5
*H*45*L*45	45	45

* All values are in mm.

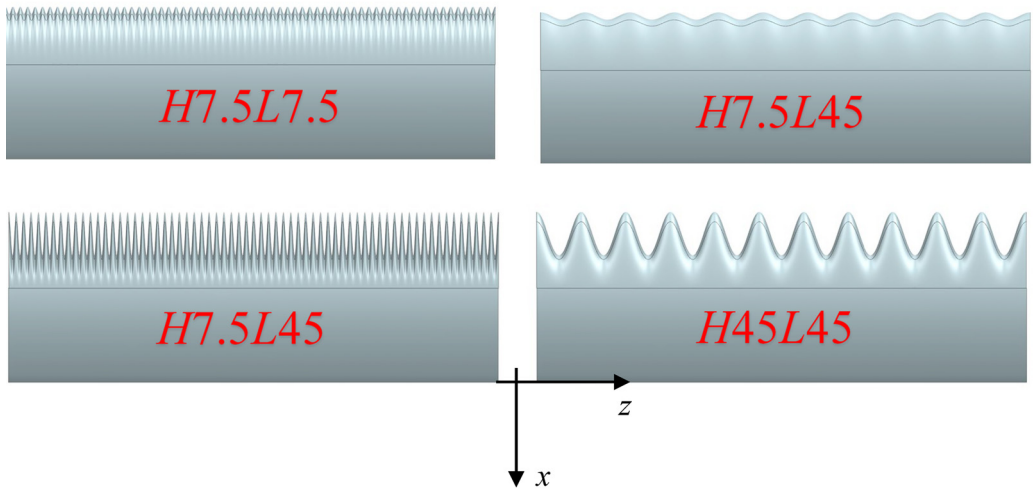

FIG. 1. (Color online) Description of the serrated leading edges and their geometries investigated in this study when viewed in the *x*–*z* plane.

aerofoil self-noise level across the entire velocity range (Vathylakis *et al.*, 2014). The aerofoil is held by two optically transparent side plates flush mounted to the lips of the nozzle at a geometrical 0° angle of attack throughout the experiments.

The far field noise was measured by an array of eight G.R.A.S. $^1/_2$-in. condenser microphones (Denmark) located at a distance of 1 m above the trailing edge at the mid-span plane of the aerofoil. The microphones are distributed across the array covering the emission angles relative to the downstream direction of the jet axis from 50° to 120°. Noise data from all microphones are acquired at a sampling rate of 40 kHz for a period of 20 s by a 16-bit analogue-digital card from National Instruments (USA). The acoustic signals are then windowed (4096 points), and Fourier transformed to calculate the power spectral density (PSD) with a 1 Hz bandwidth (dB/Hz) and a frequency resolution of 10 Hz. Using the PSD of the fluctuating pressure time history acquired from the microphones, the sound power level (PWL) per unit span can be calculated for the range of radiation angles between 50° and 120° based on a cylindrical spreading of the acoustic wave from the source.

The wake flow generated by the blunt trailing edge and the effect of different leading edge serrations on the wake vortex structures is measured by a particle image velocimetry (PIV) system. This system includes a source capable of generating a double pulse laser beam (Nd:YAG Litron Laser, United Kingdom) with the maximum pulsing frequency of 15 Hz and the maximum output energy of 135 mJ per pulse. Using cylindrical and spherical lenses, a laser sheet thickness of about 1 mm is generated. A CCD camera (TSI PowerView Plus 4MP-LS, USA) is used to capture the images of the flow domain at 16 frames/s with an output resolution of 2352×1768 pixels. Di-Ethyl-Hexyl-Sebacat (DEHS) oil was used as seeding fluid because of its good reflection characteristics at high laser intensities. The oil droplet has an average diameter of 1 μm, which was seeded via a pressurised oil chamber (TSI model 9307 Oil Droplet Generator, USA) and injected into the anechoic chamber. A conventional cross-correlation algorithm was used on a 32×32 pixel grid to calculate the velocity vectors from the peak correlation of a group of particles. The average velocity field was computed by averaging 800–1000 instantaneous velocity image maps. The aerofoil surface is painted in a matte black finish in order to minimise the laser reflection from the surface. As shown in Fig. 2, the laser sheet is projected from 0.5 m below the aerofoil toward the upward direction so that the visualised area is set on the cross-sectional *x*–*y* plane. The camera is placed perpendicular to the streamwise direction adjacent to the side plate. In this experiment, the PIV measurement is taken at two *x*–*y* planes that are aligned with the serration root and tip for each serration geometry. For every changeover of the measurement plane, the aerofoil is slid through the side holding plates and the location of the laser–camera system remains unaltered. This simple procedure can avoid the need for recalibration

https://doi.org/10.1121/10.0001377

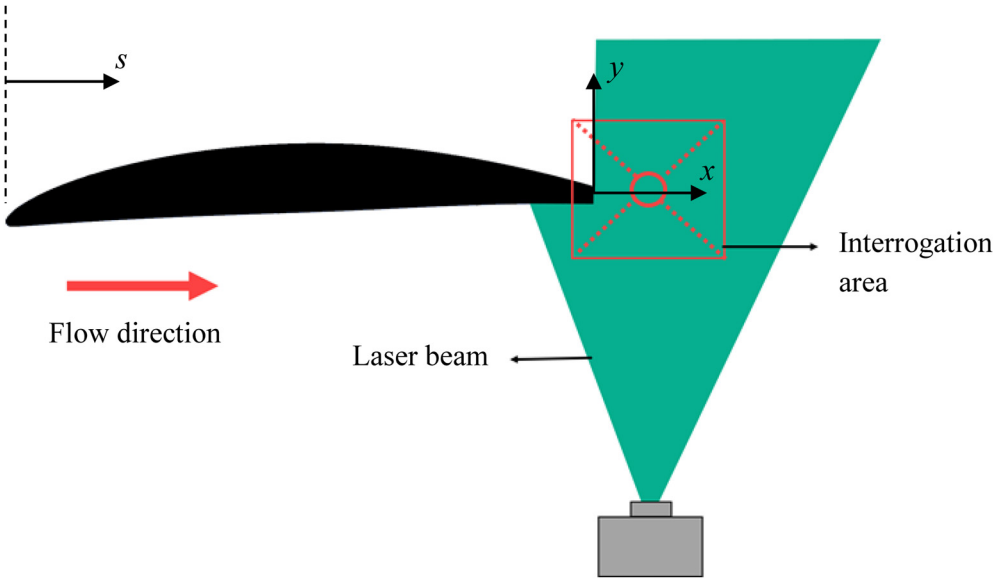

FIG. 2. (Color online) Schematic of the camera and laser positions with respect to the NACA 65(12)-10 aerofoil with a blunt trailing edge when viewed in in the x–y plane.

of the camera, while simultaneously ensuring the consistency and repeatability of the results. Time-averaged flow quantities, such as the mean and fluctuating velocity, and the energy-based coherent modes can be calculated. Note that u and v are the velocity components in the streamwise and vertical directions, respectively.

Oil flow visualisation was conducted on the aerofoil surfaces to identify the separation region and flow structures generated by the serrated leading edges. The oil mixture used in this study consists of three components: linseed oil provides the oil base of the compound, titanium dioxide is a colouring agent, and paraffin is used to control the viscosity of the compound. Care was taken to obtain an appropriate viscosity of the compound. It should be noted that the presence of the oil compound on the aerofoil surface is unlikely to affect the boundary layer significantly, especially when observing the large-scale vortex formation from the serrated leading edges.

III. WAKE ENERGY MODE DETECTION

The proper orthogonal decomposition (POD) is a mathematical linear procedure that can be used to extract the different energy modes from an ensemble of signals (Berkooz *et al.*, 1993). In the current study, the snapshots of the two-dimensional velocity fields, $\boldsymbol{v} = (x, y, t_n)$, where $n = 1, \ldots, N$, and t_n is the time of the snapshot, are acquired by the PIV. N is the total number of snapshots (800–1000 in the current work), which can be used to construct a covariance matrix C_{ij}:

$$C_{ij} = N^{-1}\left(\boldsymbol{v}(x, y, t_i), \boldsymbol{v}(x, y, t_j)\right), \tag{1}$$

where $i,j = 1,\ldots,N$.

A corresponding eigenvalue problem can be solved:

$$\mathrm{C}_{ij} l^{(i)} = \lambda_i l^{(i)}. \tag{2}$$

Since C_{ij} is symmetric, it has N real eigenvalues $\lambda_1 \geq \lambda_2 \geq \cdots \geq \lambda_N$ with the corresponding eigenvectors $\boldsymbol{l}^{(1)}$, $\boldsymbol{l}^{(2)}$,…, $\boldsymbol{l}^{(N)}$, where $\boldsymbol{l}^{(i)} = (l_1{}^{(i)}, l_2{}^{(i)}, \ldots, l_N{}^{(i)})^t$. The POD analysis gives the basis to reproduce the velocity field by the modal decomposition as a linear combination of

$$\boldsymbol{\psi}^{(i)}(x, y) = \sum_{n=1}^{N} l_n^{(i)}\, \boldsymbol{v}(x, y, t_n), \tag{3}$$

where $\boldsymbol{\psi}^{(i)}$ $(i = 1,\ldots,N)$ represents the POD-eigenmodes. Since each eigenmode contains elements of all flow structures from the whole snapshot (instantaneous velocity fields), the first mode is usually enough to capture the same structures available in the original snapshots with the most fraction of total energy, whereas the other modes may include noise. The ordering of both the eigenvalues and eigenvectors ensures that the first mode, which is of the highest energy mode, represents the large-scale coherent structure in the wake region.

IV. DISCUSSION OF RESULTS

The PWL corresponding to each serrated aerofoil, including that produced by the baseline aerofoil, is shown in Fig. 3. The noise measurement was performed for a velocity range $20 \leq U_\infty \leq 60$ m/s. For conciseness, most of the discussion on the far field and near field will focus on results measured at $U_\infty = 20$ m/s, but results obtained at other velocities will also be analysed at the relevant sections. In Fig. 3, a narrowband tonal noise is clearly discernible for the baseline aerofoil at a nondimensional frequency, Strouhal number St $(= fd/U_\infty)$ at 0.18, where f is the frequency in Hz and d is the blunt trailing edge thickness in meters. Tonal peaks observed at other velocities also adhere

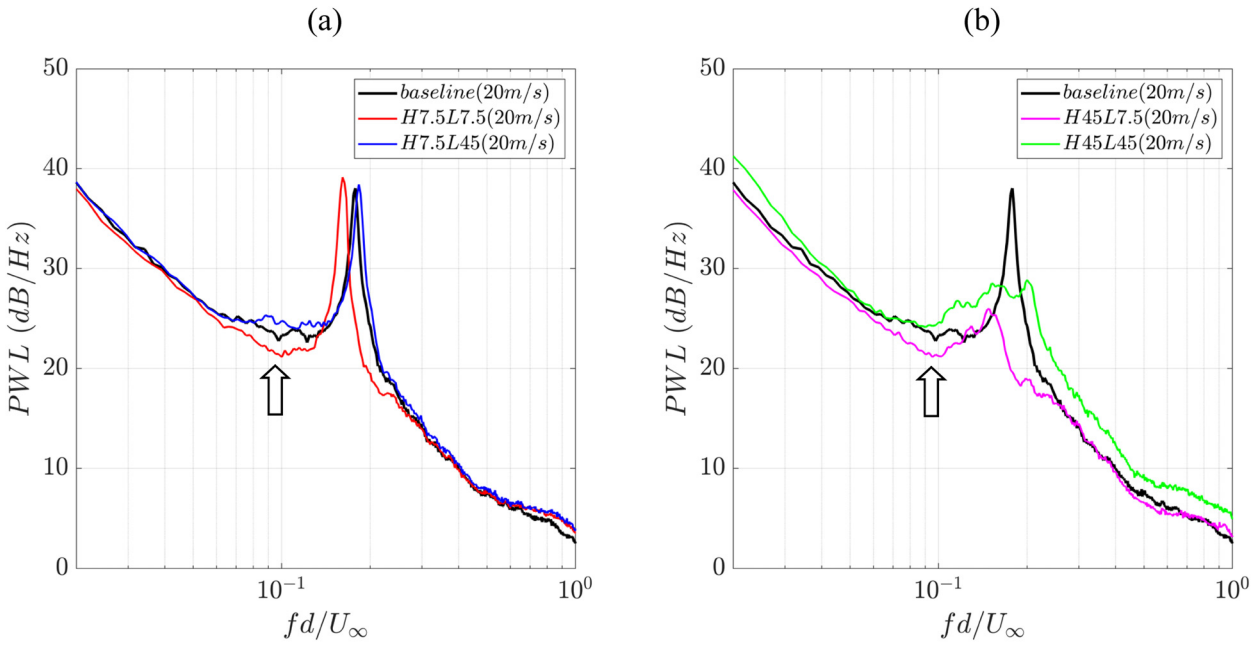

FIG. 3. (Color online) PWL (dB/Hz) radiated by the NACA 65(12)-10 with a blunt trailing edge subjected to a straight (baseline) and several serrated leading edges at $U_\infty = 20$ m/s.

to the same Strouhal number, which suggest that the narrowband tonal noise is likely to be associated with the bluntness-induced vortex shedding. Before that, however, it is necessary to investigate whether other aerofoil noise sources also contribute in the measured noise spectra.

Because the inflow turbulence intensity is very low at $<0.1\%$, the leading edge noise is not expected to be significant in the current study. However, laminar instability tonal noise will be a dominant feature under the similar combination of the Reynolds number and angle of attack for the untruncated NACA 65(12)-10 aerofoil, i.e., when the trailing edge is sharp (Chong *et al.*, 2018). The presence of a laminar boundary layer separation near the trailing edge is widely considered a prerequisite for an effective radiation of laminar instability tonal noise owing to its prominent role in the amplification of the incoming Tollmien-Schlichting waves (Nash *et al.*, 1999; Chong and Joseph, 2009). Using oil flow visualisation, Chong *et al.* (2018) observed a laminar separation of the boundary layer at $s/C \approx 0.80$ on the suction surface of the NACA 65(12)-10 (sharp trailing edge) with no reattachment, which is shown in Fig. 4. They established that the characteristic of the laminar instability tonal noise is predominantly governed by this separation region.

In a separate test, the boundary layer tripping element was placed on the suction surface of the NACA 65(12)-10 with a sharp trailing edge, one at a time, at $s/C = 0.99$, 0.98, 0.97, and so on, up to $s/C = 0.87$. The premise of this test is that the boundary layer downstream of the tripping element will be instantaneously disturbed, and this will facilitate the study of the sensitivity of the separation length to the radiated laminar instability tonal noise. The most upstream tripping element is placed at $s/C = 0.87$ as this coincides with the blunt trailing edge of the truncated NACA 65(12)-10 aerofoil. Figure 5 shows the sound pressure level (SPL; dB/Hz reference to 2×10^{-5} Pa) of the far field noise measured at 90° polar angle, 1 m from the trailing edge at mid span, and at $U_\infty = 20$ m/s. When the tripping element is placed at the most downstream location at $s/C = 0.99$, this would entail the least destruction of the separation length. Therefore, the classical feature of a broadband–hump embedded with the high amplitude discrete tones can be identified. This causal relationship is continuously manifested when the tripping element moves toward upstream, where both the broadband–hump and discrete tones are found to slowly diminish. The noise spectrum at a tripping location of $s/C = 0.87$ has virtually no tonal

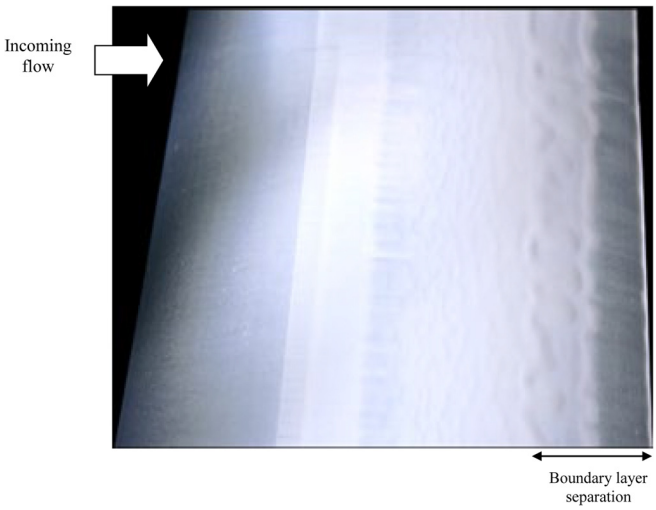

FIG. 4. (Color online) Surface oil flow visualisation (suction side) for the NACA 65(12)-10 aerofoil with a straight leading edge and sharp trailing edge. $U_\infty = 24$ m/s and angle of attack = 0°.

https://doi.org/10.1121/10.0001377

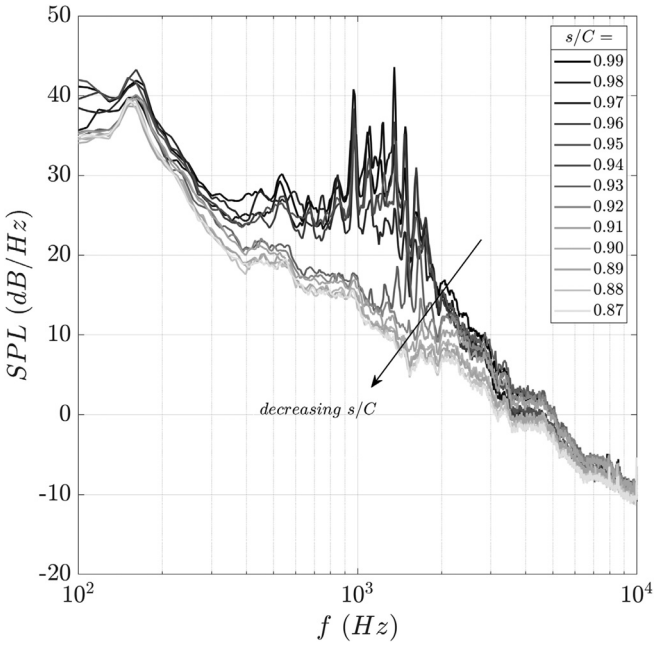

FIG. 5. Sound pressure level (SPL; dB/Hz) radiated by the NACA 65(12)-10 with a straight leading edge and sharp trailing edge, subjected to different boundary layer tripping locations (s/C) at the suction side at $U_\infty = 20$ m/s.

characteristic left, although a certain broadband level of the laminar instability noise might still be present as there is a remnant of separation region between $s/C = 0.80$ and 0.87.

For the aerofoil with a blunt trailing edge, the replacement of the straight leading edge with both the *H*7.5*L*7.5 and *H*7.5*L*45 serrated leading edges offers no noticeable reduction in the narrowband tonal noise level as demonstrated in Fig. 3(a). Nevertheless, a closer examination of the PWL spectra reveals an interesting phenomenon for the *H*7.5*L*7.5 serration. The tonal peak is found to shift slightly towards a lower Strouhal number (St = 0.16) compared to the baseline case (St = 0.18). Because of the global frequency shifting, it gives an appearance that the noise reduction has been achieved against the baseline spectrum at a frequency range close to the tonal component. Special attention is paid to the noise reduction at a finite frequency range lower than the main tone, which is marked by an arrow in Fig. 3(a). For identification purposes in the remainder of this paper, this particular frequency range is referred to as the sub-vortex shedding tone (VST).

Although a low *H* in the serration seems to exert little influence on the bluntness-induced tonal peak, applying a larger *H* (*H*45*L*7.5 and *H*45*L*45) is more successful in the reduction of the tonal peak level as demonstrated in Fig. 3(b). In addition, both the large *H* serrations seem to broaden the tonal component, which could imply the weakening of coherent structures in the wake. This will be discussed further in Sec. IV A. The serrated configuration that provides the largest noise reduction, where up to 10 dB can be achieved, is the *H*45*L*7.5. Interestingly, this configuration also exhibits the global Strouhal number shifting in the PWL in a similar fashion as the *H*7.5*L*7.5 described earlier, resulting in noise reduction at the sub-VST frequency (also marked by an arrow). However, as will be discussed later, noise reduction at this frequency region is not because of the frequency shifting.

As a summary, employing the serrated leading edge can manipulate the self-noise radiation of an aerofoil with a blunt trailing edge in two ways. First, the serration amplitude *H* is the primary geometrical parameter for the suppression of the bluntness-induced vortex shedding tonal noise. Second, the serration wavelength *L*, when small enough, can cause a global frequency shifting of the tonal noise and a reduction of noise at the sub-VST frequency. This feature does not seem to be sensitive to the level of *H*. In what follows, the mechanisms for the above two features will be investigated in detail.

A. Effect of the leading edge serration amplitude *H* on the bluntness vortex shedding tonal noise

Previously, the bluntness-induced vortex shedding was deduced as the main mechanism for the generation of tone noise and the Strouhal number dependency in the acoustic spectra. The vortex shedding can be described as an unstable fluid motion and when viewed in phase-locked time frames, it would appear as stationary. Using the POD method described earlier, the largest energy-containing coherent structures in the velocity field can be reproduced vividly by the first eigenmodes in *u* and *v*.

Figure 6 shows the POD-eigenmodes of the highest energy for both *u* and *v* velocity fields produced by the baseline, *H*7.5*L*7.5 and *H*45*L*7.5 aerofoil. For the baseline case, the characteristics of the coherent shedding are well represented. Overall, the eigenmodes display a slight downward trajectory due to the asymmetric nature of the NACA 65(12)-10. The structure energy content decreases while propagating downstream. The eigenmodes in *u* exhibit a quadrupole-like pattern associating with a complete shedding phase, whereas the eigenmodes in *v* alternate along the streamwise direction. It can be observed that the dominant *v* eigenmodes always situate at the foci of the quadrupole for the *u* eigenmodes, which has no energy presence. This demonstrates that the downwash and upwash phases of the shedding event are associated with minimal changes in the streamwise velocity. The appearance of such a pattern in the wake flow is indicative of the footprint of a vortex shedding phenomenon where the streamwise velocity components in both the streamwise and normal directions alternatively increase and decrease. Based on the POD-eigenmodes of the highest energy, the wavelength of the successive shedding structure is found to be about 20 mm. Assuming that the vortical structures propagate at 70% of the freestream velocity, it would result in a shedding frequency of 700 Hz. This is indeed very close to the acoustical frequency of the radiated tone noise at 715 Hz.

The POD analysis now focuses on the velocity fields in the presence of serrated leading edges. It is worth reminding that the baseline and all the serrated leading edges

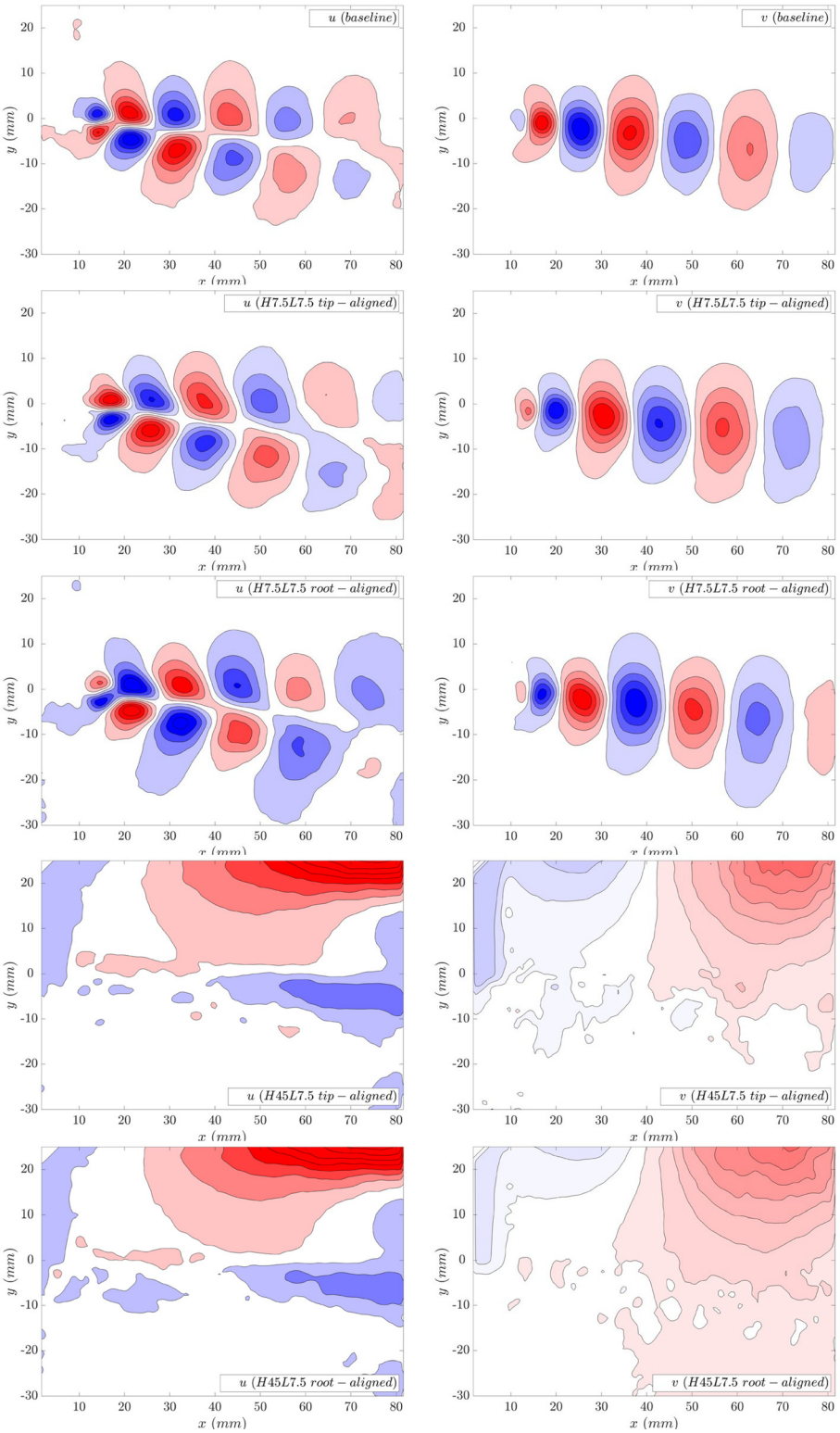

FIG. 6. (Color online) Comparison of the most dominant POD modes in u and v for the baseline, $H7.5L7.5$ and $H45L7.5$ leading edges at $U_\infty = 20$ m/s.

investigated here have the same type of blunt trailing edge. As a result, any differences in the flow field downstream of the aerofoil are solely due to the modification of boundary layers by the serrated leading edges. The flow field is examined in two cross-sectional x–y planes, where one is aligned with the serration tip and another is aligned with the serration root. The first impression of the velocity eigenmode distributions produced by the $H7.5L7.5$ is that footprints of vortex shedding still strongly persist in the wake flow. Indeed, it is manifested in the far field spectra, where the level of the bluntness-induced tone noise is not affected by the $H7.5L7.5$ serrated leading edge. However, a shift in the tone frequency is also observed, and this leads to a lower Strouhal number for the tone ($\mathrm{St} = 0.16$). The spatial compactness of the dominant eigenmodes for both the u and v across the tip-aligned and root-aligned planes is slightly

https://doi.org/10.1121/10.0001377

loosened compared to those produced by the baseline counterpart. This means that the *H*7.5*L*7.5 serrated leading edge can slightly disrupt the shedding cycle of the wake coherent structures and the radiated tone frequency. Another subtle difference can be observed for an offset in the spatial distributions of both u and v between the tip-aligned and root-aligned dominant eigenmodes. This can be interpreted that the wake vortex shedding becomes undulated in the spanwise direction in accordance to the wavelength L of the leading edge serration. Taking an average value of 21.7 mm for the wavelength of the successive shedding structure between the tip-aligned and root-aligned planes and, again, assuming a convective velocity of $0.7\,U_\infty$, the shedding frequency pertaining to the *H*7.5*L*7.5 aerofoil is 645 Hz. This rough estimation matches well against the corresponding radiated tone frequency, which is measured at 640 Hz.

Evidence suggests that the level of deviation of the tone frequency produced by a low-H serrated leading edge is dictated by the level of L. When L is large, the wake vortex shedding will be less undulated in the spanwise direction, thus, adhering more to the original tone frequency (see the PWL spectra by the *H*7.5*L*45 leading edge). This leads to a suggestion that, as far as a sufficiently low-wavelength serrated leading edge (e.g., *H*7.5*L*7.5) is concerned, an effective trailing edge bluntness might be able to supersede the physical geometry d when defining the tone frequency in the Strouhal number.

To explore this option, an attempt was made to redefine the Strouhal number by replacing the characteristic length scale with the near wake displacement thicknesses, which can be obtained from the PIV data. For the serrated aerofoil, the averaged near wake displacement thickness between the tip-aligned and root-aligned planes is taken. However, the new Strouhal numbers describing the tonal peaks between the baseline and serrated aerofoils are still not compatible. This is because the three-dimensional nature of the hydrodynamic field at the trailing edge of a serrated aerofoil would undulate the wake vortex shedding periodically in the spanwise direction. This will certainly make it difficult to define a true characteristic hydrodynamic length scale for the Strouhal number, especially the tonal peaks. Therefore, a simple geometrical bluntness d is still adopted in the current paper when defining the Strouhal number.

When the serration amplitude H is increased, such as in the *H*45*L*7.5 case, a more dramatic change in the wake flow and the radiated far field can be observed. Applicable to both the tip-aligned and root-aligned planes, the wake flow no longer exhibits any recognisable eigenmodes in u and v that resemble a vortex shedding in Fig. 6. Rather, the most energetic structures in the figure are associated with the shear layers produced by the nozzle (only those produced by the top lip are shown in Fig. 6). The lack of a coherent eigenmode in the wake flow also correlates well with the much reduced turbulence intensity level of the transverse velocity component $v_{\mathrm{rms}}/U_o(x)$ in Fig. 7, which could be used to indicate the level of vortex shedding. Note that v_{rms} is the root-mean-square of the v, and $U_o(x)$ is the local free stream velocity at the wake region. These hydrodynamic behaviours translate into a significant reduction but not a complete suppression of the radiated tone noise level. This causes an appearance of a broadened tonal hump with reduced noise level in the acoustic spectrum [Fig. 3(b)].

For the *H*45*L*45 leading edge, the radiated noise is also characterised by a transition from sharp tone to broadened

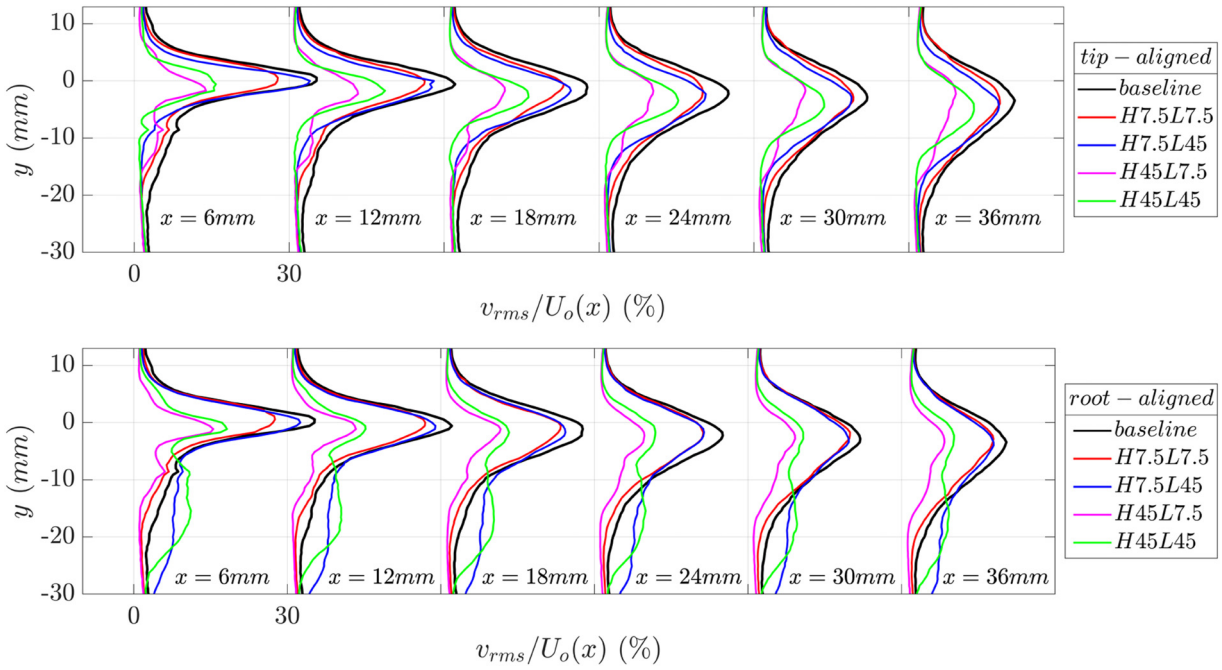

FIG. 7. (Color online) Streamwise evolution of the transverse component of velocity fluctuations in the wake by the baseline leading edge and different serrated leading edges at $U_\infty = 20$ m/s.

tonal hump, although, at a larger acoustic level than the *H*45*L*7.5 leading edge. The wake pertaining to the *H*45*L*45 leading edge, although not shown here, is also deprived of the coherent eigenmodes in both u and v. The corresponding $v_{\mathrm{rms}}/U_o(x)$ field in Fig. 7 possesses a slightly larger fluctuating level than the *H*45*L*7.5, but still maintains an overall much lower level than those produced by the baseline and low-*H* serrated leading edges (*H*7.5*L*7.5 and *H*7.5*L*45).

B. Investigation of the noise origin at the sub-VST frequency

The mechanism responsible for the reduction of noise at the sub-VST frequency by the serrated leading edges is the subject of investigation here. As the name already indicated, a candidate for the noise source could be related to the bluntness-induced vortex shedding in the wake. However, this conjecture can be dismissed easily due to the fact that the radiated noise at the sub-VST frequency range can only be reduced by the low-value serration wavelength L, regardless of the level of serration amplitude H (Fig. 3). This contradicts the previous findings in which a large H is required to suppress the bluntness-induced vortex shedding. Therefore, it is unlikely the main reason.

Another possible candidate for the noise generated at the sub-VST frequency is related to the acoustical scattering of the boundary layer instability wave after interaction with the separation bubble near the trailing edge. If this conjecture were true, it would mean that the acoustic spectra pertaining to the aerofoil with a blunt trailing edge should contain two tonal components: one refers to the bluntness-induced vortex shedding tonal noise and another is the laminar boundary layer instability tonal noise. Although it is not immediately clear from the PWL spectra in Fig. 3 ($U_\infty = 20$ m/s), the two tonal components could be separated farther apart in the frequency domain, and thus more distinguishable from each other, if they exhibit different velocity dependency laws. Figure 8(a) shows the PWL spectra produced by the baseline aerofoil with a blunt trailing edge at $20 \leq U_\infty \leq 60$ m/s. From Fig. 8(a), each acoustic spectrum is characterised by the appearance of a massive tone 15–20 dB larger than the otherwise unperturbed one. These tones are marked by red-coloured solid line arrows in Fig. 8(a). They persist tenaciously throughout the velocity range with their peak frequencies increasing with the velocity. Interestingly, as the velocity increases, a smaller tonal-hump in the acoustic spectra, which are marked by the blue-coloured dashed arrows, begins to appear prominently below the main tone frequency. Figure 8(b) shows the variations of the main tone frequency and the smaller tonal-hump frequency against the velocity. The main tone frequency is found to scale with $U_\infty{}^{1.0}$, which perfectly illustrates the validity of the Strouhal number scaling for the vortex shedding tonal noise. The peak frequency of the tonal-humps at the sub-VST region is analogous to the dominant discrete frequency $f_{n\text{-max}}$, described in Chong and Joseph (2012). They are found to scale with $U_\infty{}^{0.75}$ with at least one ladder-jump occurring within $20 \leq U_\infty \leq 60$ m/s. These important observations not only reaffirm the early dismissal of the bluntness-induced vortex shedding being responsible for the noise radiation at the sub-VST frequency, but, also more interestingly, the $U_\infty{}^{0.75}$ scaling for the dominant discrete frequency matches close to the scaling law of the discrete tones for the laminar aerofoil instability tonal noise at 0.8 (Chong and Joseph, 2009). This comparison suggests that the noise radiation at the sub-VST frequency could be related to the boundary layer instability mechanism.

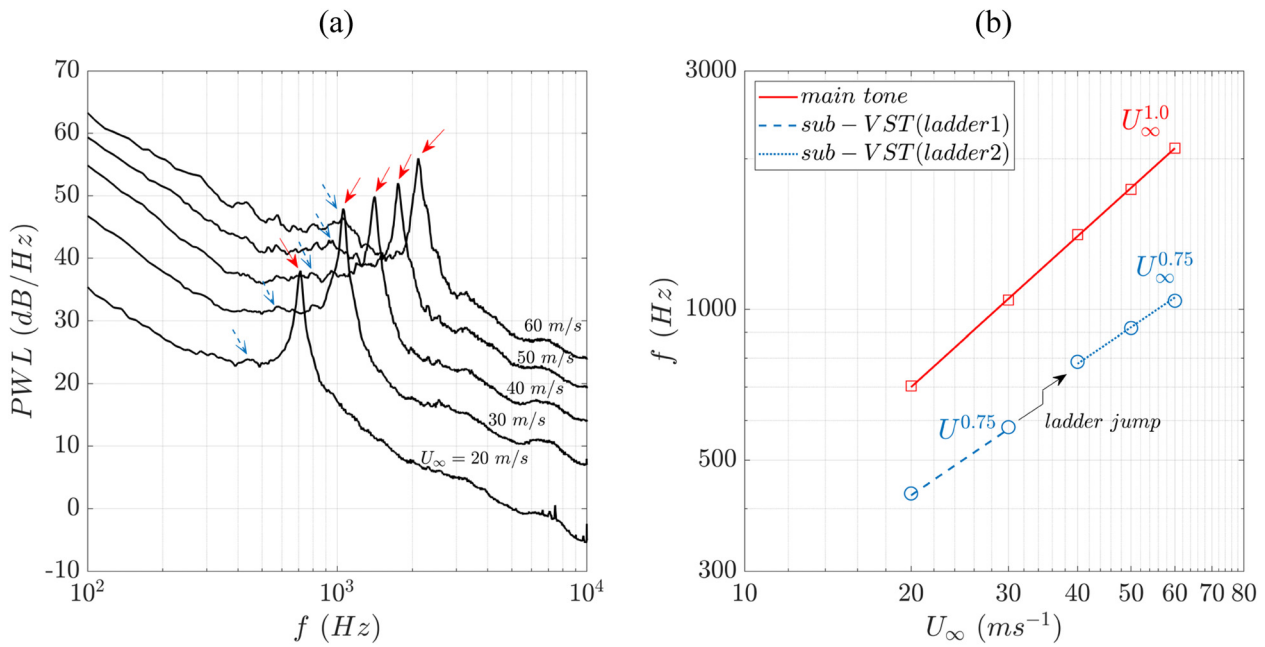

FIG. 8. (Color online) (a) PWL (dB/Hz) radiated by the NACA 65(12)-10 with a blunt trailing edge subjected to a straight (baseline) leading edge between 20 m/s $\leq U_\infty \leq$ 60 m/s. (b) Variations of the main tone and sub-VST frequencies against inflow velocities.

https://doi.org/10.1121/10.0001377

Although noise radiation at the sub-VST frequency is now confirmed to be unrelated to the bluntness-induced VST, the term "sub-VST" is retained in the subsequent discussion whenever referring to that specific frequency range.

To establish the link between the tonal-hump at the sub-VST frequency and the boundary layer instability firmly, the SPL produced by the NACA 65(12)-10 with a sharp trailing edge at $U_\infty = 20$ m/s, presented earlier in Fig. 5, can be re-examined. For this aerofoil with a sharp trailing edge, the suction side boundary layer is the least perturbed by the tripping element when placed at $s/C = 0.99$ because it is already very close to the trailing edge. The corresponding acoustic spectrum exhibits a dominant tonal noise (with multiple discrete tones embedded) at $300 \leq f \leq 3000$ Hz, which would have covered the radiated tonal-hump at the sub-VST. Therefore, the tonal-hump at the sub-VST is almost certainly the boundary layer instability tonal noise based on the familiar characteristics. From now on, this will be called the "instability tonal-hump" in order to distinguish it from the bluntness-induced tonal noise.

When the tripping element is moved upstream, from the acoustical perspective, this is equivalent to creating a truncated trailing edge, but without the presence of the bluntness-induced vortex shedding tonal noise or a significant turbulent broadband noise radiation. Moving the tripping element upstream from near the trailing edge $s/C = 0.99$ to $s/C = 0.87$ (location that coincides with the blunt trailing edge), both the dominant tonal-hump (i.e., boundary layer instability noise) and the discrete tones begin to subside in the SPL, but the characteristic frequencies remain relatively unchanged. The above phenomenon is mostly likely due to the weakened amplification of the boundary layer instability by the shortened separation bubble length because of the upstream placement of the tripping element. This would explain the not-so-obvious boundary layer instability tonal noise radiated at the sub-VST frequency region of the blunt trailing edge aerofoil, especially at low inflow velocity. Some surface oil flow visualisation results will be presented in Sec. IV C to complement this observation.

C. Effect of the leading edge serration wavelength *L* on the instability tonal-hump reduction at the sub-VST frequency

The PWL spectra in Fig. 3 establish that the instability tonal-hump radiation at the sub-VST frequency can only be manipulated effectively when a large number of streamwise vortices generated by the leading edge serration is provided. This implies that it is more effective if a small serration wavelength L is used. The basis of this phenomenon stems from the interaction between the streamwise vortices and the separation bubble that ultimately manipulates the noise radiation. Figure 9 summarises results from the oil flow visualisation for the *H*7.5*L*7.5, *H*7.5*L*45, *H*45*L*7.5, and *H*45*L*45 serrated leading edges. Note that these results had been published earlier in Chong *et al.* (2018), where the serrated leading edges were formed by the cut-in approach, and a sharp trailing edge was used. Despite the geometrical differences, it is still valid to apply the results in Fig. 9 to extract the mechanism of noise reduction at the instability tonal-hump by certain types of the serrated leading edge. The corresponding oil flow visualisation for the straight leading edge aerofoil had been shown earlier in Fig. 4, which established that boundary layer separation starts at $s/C \approx 0.80$ and without reattachment. For the truncated aerofoil, the blunt trailing edge would have been located at $s/C = 0.87$, which provides an important implication that a separation region covering $\Delta s/C \approx 0.07$ (10.5 mm) still contributes in the radiation of the instability tonal noise. The reduced separation length for the truncated aerofoil might be the reason for a subtle noise level of the instability tonal-hump at the sub-VST frequency observed in Sec. IV B.

By focusing on the serrated leading edges with a large L (*H*7.5*L*45, *H*45*L*45), it is clear that the emanated streamwise vortical structures are too far apart from each other in the spanwise direction, such that some distinctive flow patterns, for example, the Ω structures for the *H*7.5*L*45 case in Fig. 9, can be formed. As a result, pockets of the separated region are still prominent near where the blunt edge is located ($s/C = 0.87$). This ultimately facilitates the radiation of the instability tonal-hump in a similar fashion as their baseline aerofoil counterpart. On the other hand, when the serrated leading edges of small L are used (*H*7.5*L*7.5, *H*45*L*7.5), the close proximity of each streamwise vortical structure may encourage mutual induction against each other, thus, enhancing the suppression of the separation bubble. It is clear from the flow visualisation images that the region at $s/C = 0.87$ is occupied almost entirely by the streamwise vortices in such a way that the noise level pertaining to the instability tonal-hump is reduced very significantly.

To ensure that the mechanisms described above are also applicable to other inflow velocities, Fig. 10 shows the PWL spectra produced by the four different serration models and the baseline when U_∞ is increased to 30 and 60 m/s. The capability of the *H*7.5*L*7.5 and *H*45*L*7.5 (and inability of the *H*7.5*L*45 and *H*45*L*45) to suppress the instability tonal-hump radiation at the sub-VST frequency continues to manifest in the acoustic spectra. In terms of the suppression of the bluntness-induced tone noise, *H*45*L*7.5 and *H*45*L*45 (i.e., large H) remain the optimal choices.

Further investigation of the acoustical field for the *H*45*L*45 leading edge, which entails a large serration amplitude and wavelength, reveals different spectral characteristics in four nondimensional frequency zones when compared to the baseline aerofoil:

(1) (*Zone* 1: $0.09 < \mathrm{St} < 0.16$) The *H*45*L*45 leading edge seems to enhance the instability tonal-hump radiation at the sub-VST. Note that the upper and lower limits of the Strouhal number range are not universal against the inflow velocity because the length scale of trailing edge bluntness cannot be used to describe the instability noise. The values provided inside the bracket are therefore indicative only.
(2) (*Zone* 2: $0.16 \leq \mathrm{St} \leq 0.19$) The otherwise prominent bluntness-induced VST produced by the baseline aerofoil is suppressed.

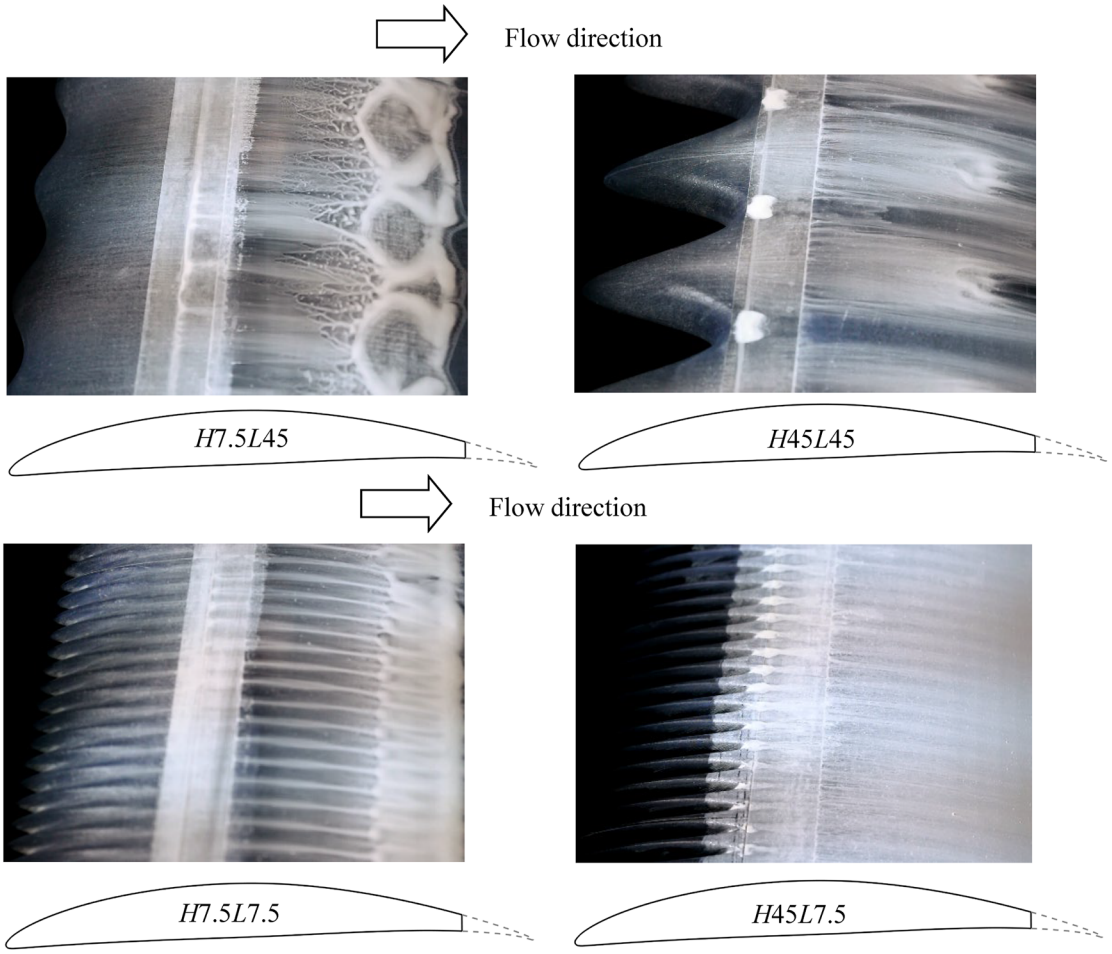

FIG. 9. (Color online) Surface oil flow visualisation (suction side) for the NACA 65(12)-10 aerofoil with serrated leading edge. $U_\infty = 24$ m/s and angle of attack $= 0°$.

(3) (*Zone* 3: St $= 0.2$) The bluntness-induced VST reemerges. This scenario is especially prominent at a higher inflow velocity. Also note that the Strouhal number in this case is slightly higher than that produced by a baseline aerofoil at St $= 0.18$.
(4) (*Zone* 4: St > 0.2) Broadband noise level produced by the *H*45*L*45 serrated leading edge is consistently larger than the baseline aerofoil.

In *zone* 1, a reference can be made against the oil flow results in Fig. 9 for the *H*45*L*45 leading edge. The darker, wedge-shaped region originating from the serration roots, as well as the pockets of flow separation near the trailing edge, could provide an enhanced interaction with the Tollmien-Schlichting instability waves to increase the level of tonal-hump radiation. Acoustical characteristics in *zone* 2 are the result of wake manipulation by a large amplitude serrated leading edge that can produce a spanwise array of strong streamwise vortices. However, the reemergence of the bluntness-induced tone in *zone* 3 also denotes that the spanwise arrays of streamwise vorticity are too far apart from each other as the result of the large serration wavelength such that a significant compartmentalisation of the vortex shedding occurs in the spanwise direction. As a result, the pockets of the wake region that do not interact with the array of streamwise vortices become a weak source for the bluntness-induced tonal noise radiation. A possible mechanism for the broadband noise increase in *zone* 4 will be discussed in Sec. IV D concerning the wake flow manipulation by the serrated leading edges.

D. Wake manipulation by the serrated leading edges

The analysis, thus far, suggests that implementing a particular type of serrated leading edge (i.e., *H*45*L*45), despite being effective in the suppression of the bluntness-induced tonal noise, also produces an unwanted by-product in the form of a broadband noise increase at high frequency. This extraneous noise source should be caused by the three-dimensional perturbations to the boundary layer and/or wake owing to the large amplitude and wavelength of the serrated leading edge. To investigate this in more detail, Fig. 11 shows the u profiles downstream of the blunt trailing edge at $x = 2, 6, 10, \ldots, 22$ mm produced by the baseline and four serrated leading edges aligned with both the serration tip and serration root at $U_\infty = 20$ m/s. The readers are reminded that x refers to the streamwise distance from the blunt trailing edge. With $y = 0$ representing the midpoint of

https://doi.org/10.1121/10.0001377

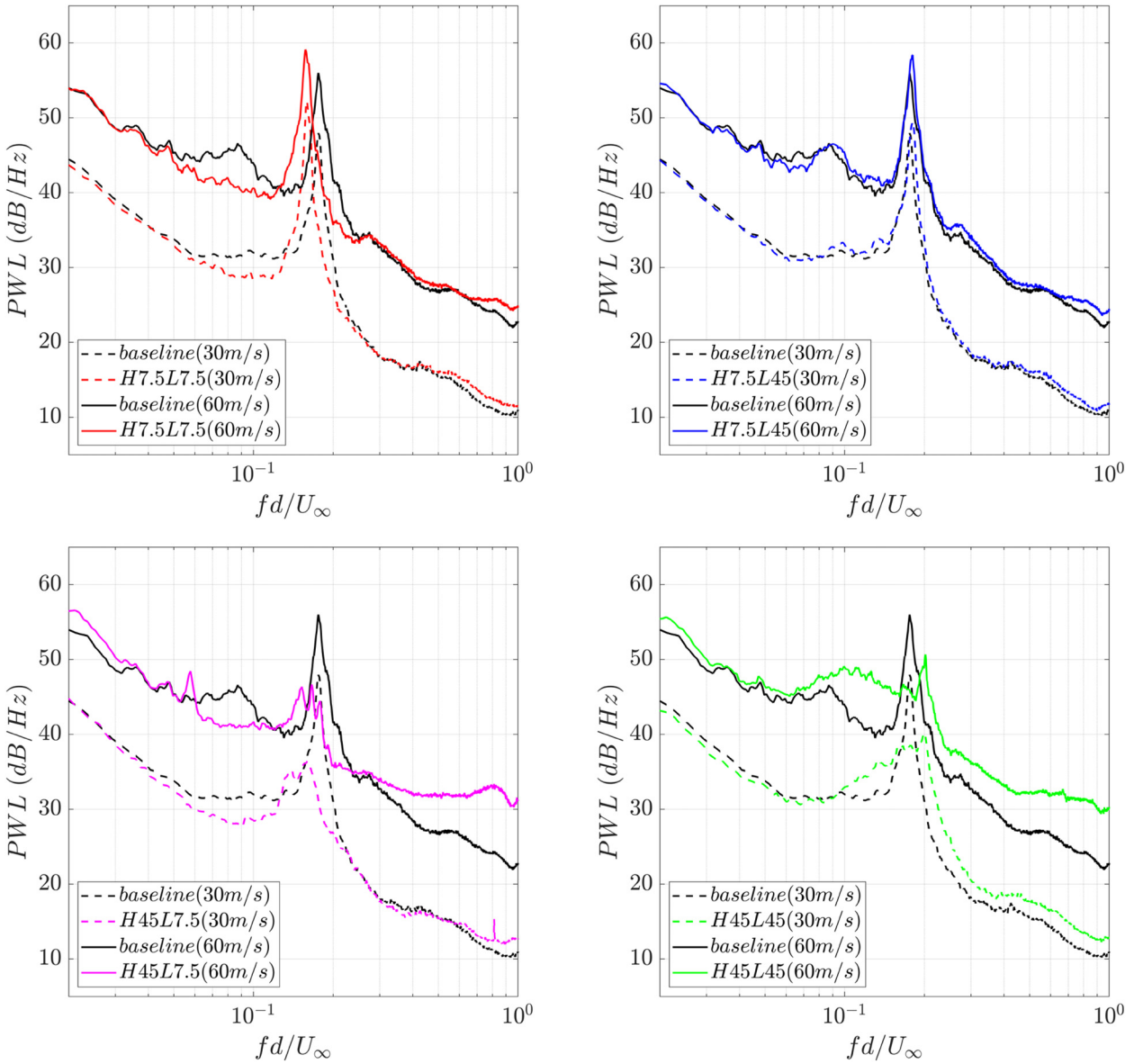

FIG. 10. (Color online) Comparison of the PWL (dB/Hz) radiated by the NACA 65(12)-10 with a blunt trailing edge between the straight (baseline) leading edges and different serrated leading edges at $U_\infty = 30$ and 60 m/s.

the blunt face at the trailing edge, all the presented velocity profiles point toward a thicker shear layer at the aerofoil's pressure side than that at the suction side. The wake propagation is slightly tilted downward following the camber line of the aerofoil.

The first impression from Fig. 11 is that the u profiles produced by the baseline and $H7.5L7.5$ are relatively similar, except that the level of the velocity deficit by the serrated case is slightly larger for both the tip-aligned and root-aligned planes. The $H7.5L45$ serrated leading edge, however, exhibits different velocity patterns when compared to the baseline aerofoil. For the u profile aligned with the tip of the $H7.5L45$ serrated leading edge, the shear layer thickness at the pressures side appears to be smaller than the baseline, where the velocity profile is also fuller, especially further downstream. For the u profile aligned with the root of the $H7.5L45$, a phenomenon occurs at the pressure side in which an additional free shear layer is produced atop the wake shear layer of the aerofoil. The opposite trend of the u profiles at the pressure side of $H7.5L45$ demonstrates a spanwise modulation of the streamwise velocity acceleration and deceleration that are, respectively, aligned with the serration tips and roots, thus, providing a stretching mechanism to produce discrete streamwise vorticity components. It should be noted that for the $H7.5L7.5$ case discussed earlier, the lack of variation in velocity profiles at the trailing edge and wake regions despite possessing the same serration amplitude as the $H7.5L45$ is due to an early amalgamation of the relatively weak streamwise vortices generated at the leading edge with a much smaller serration wavelength.

For the baseline aerofoil, wake vortex shedding is only formed after the rollup of the separating shear layers at a

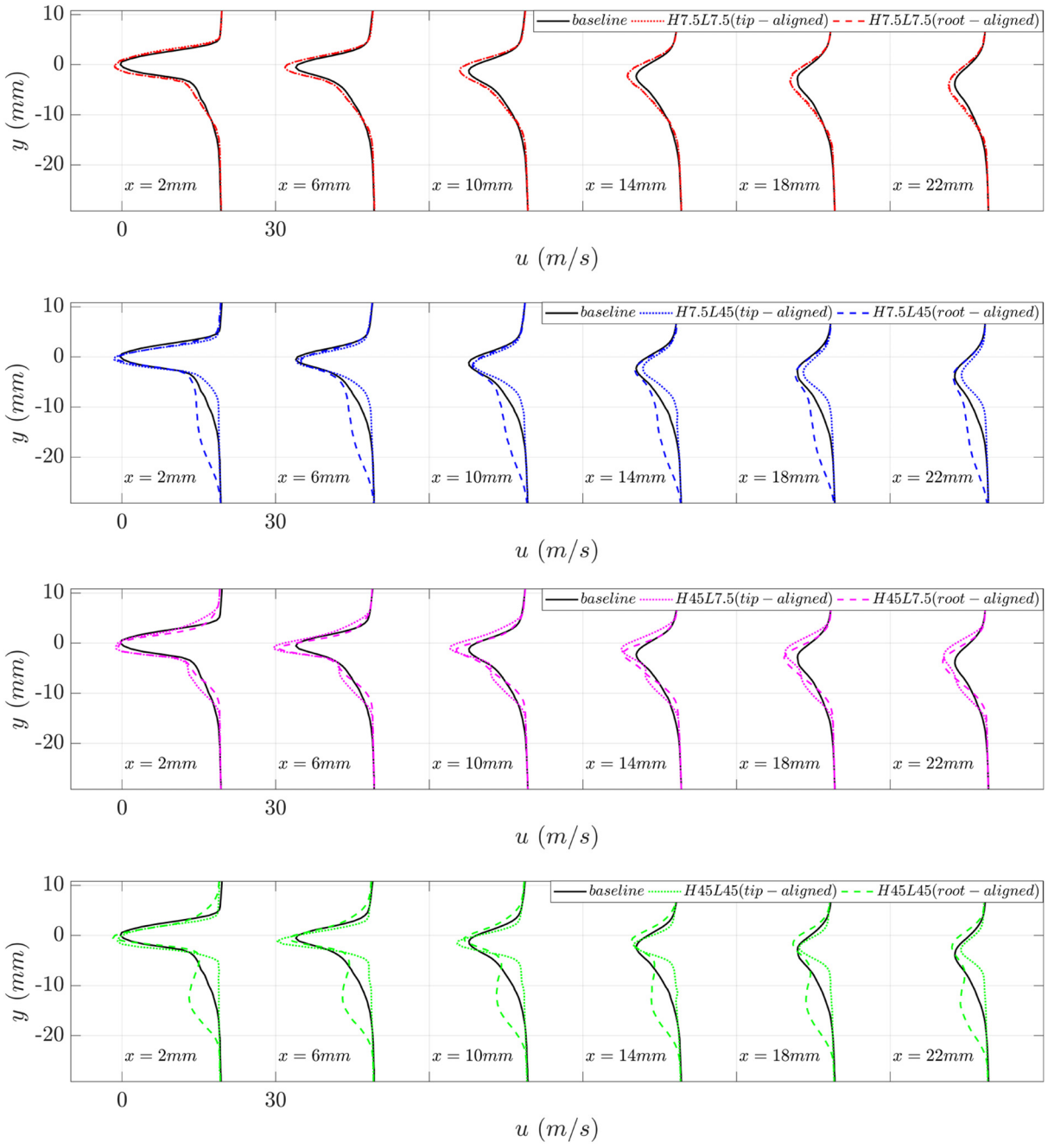

FIG. 11. (Color online) Streamwise evolution of the mean wake velocity profiles by the baseline leading edge and different serrated leading edges at $U_\infty = 20$ m/s.

certain distance downstream of the blunt trailing edge (Al-Sadawi *et al.*, 2019). By using a large serration amplitude and low serration wavelength at the leading edge, e.g., the *H*45*L*7.5 case, it becomes the most effective in the reduction of the bluntness-induced tonal noise. The mechanism is related to the injection of the closely packed spanwise array of relatively strong streamwise vorticity to disrupt the upper and lower separating shear layers and then suppress the coherent formation of vortex shedding. This process will delay the flow mixing between the upper and lower shear layers, thereby resulting in a larger level of the wake-deficit pertaining to the *H*45*L*7.5 serrated leading edge in planes that both align with the tip and root. The inflectional point can be observed for the velocity profiles at the pressure side aligning with the tip of the serrated leading edge, indicating the presence of an additional free shear layer instability locally. On the contrary, inflectional velocity profiles pertaining to the free shear layer instability are switched to the plane aligning with the root of the *H*45*L*45 serrated leading edge at the pressure side. The switching results in a much fuller velocity profile at the serration tip-aligned plane. Nevertheless, such a pattern in the spanwise modulation is quite consistent with the *H*7.5*L*45 case discussed earlier in which both share the same serration wavelength.

https://doi.org/10.1121/10.0001377

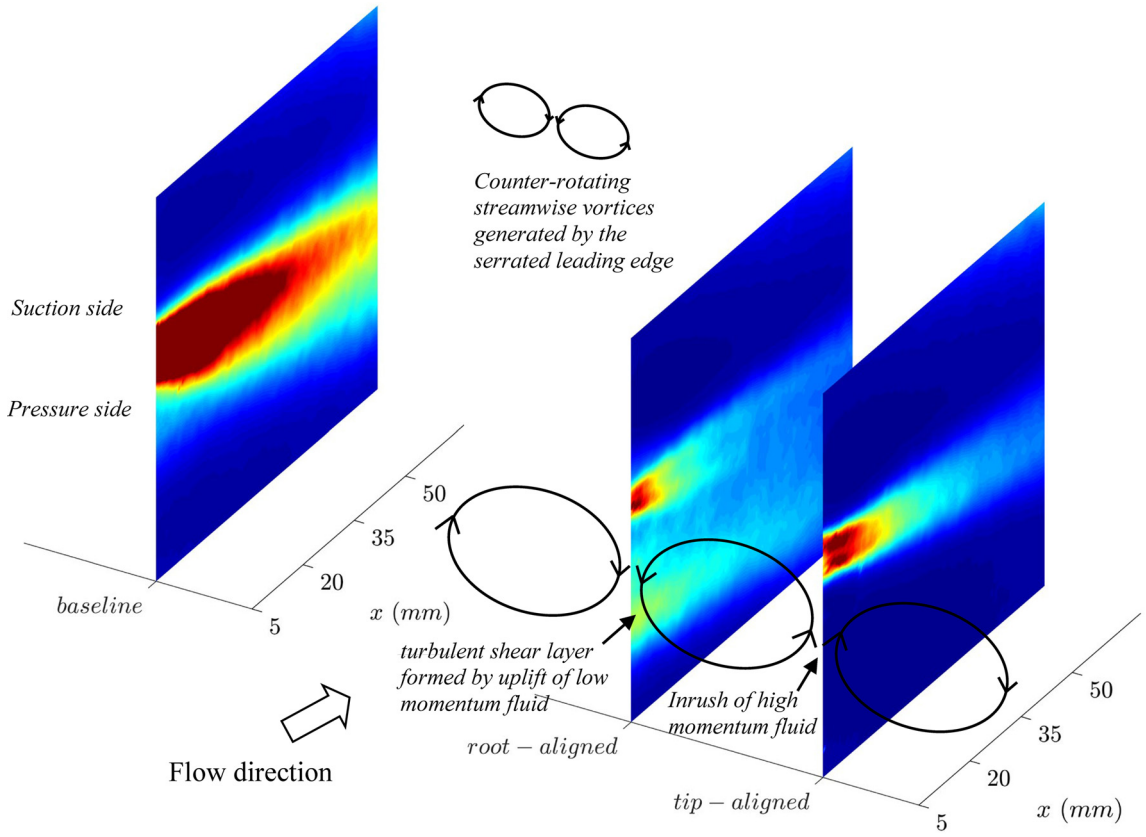

FIG. 12. (Color online) Contours of two-dimensional turbulent kinetic energy (TKE) of the wake produced by the baseline and *H*45*L*45 leading edges at $U_\infty = 20$ m/s.

Based on the velocity profiles discussed above, especially for the *H*45*L*45 case, it is plausible to conclude that distinct and mutually counter-rotating streamwise-oriented vortex structures exist at the trailing edge. To illustrate this, Fig. 12 shows the contours of the two-dimensional turbulent kinetic energy (TKE) of the wake flow, which is defined by $\text{TKE} = \frac{1}{2}\{\overline{(u')^2} + \overline{(v')^2}\}$. The planes are aligned with both the tip and root of the *H*45*L*45 serrated leading edge. The TKE contour for the baseline aerofoil is also included in Fig. 12 for comparison. It is clear that the significant level of TKE downstream of the blunt trailing edge is created by the vortex shedding. Although the mean square velocity fluctuation in the z-direction has been omitted in the definition of TKE here, the presentation of the baseline case should still be reasonably accurate because the spanwise velocity fluctuation is not expected to be significant for the vortex shedding.

In comparison, the TKE level pertaining to the *H*45*L*45 case is much lower for both the tip-aligned and root-aligned planes owing to the suppression of the bluntness-induced coherent structures in the wake by the counter-rotating streamwise vortex structures. In what follows, discussion of these counter-rotating streamwise vortex structures will focus on the field of view in reference to the aerofoil pressure side only. Therefore, when the flow direction is directed toward ($\rightarrow +y$) or away ($\rightarrow -y$) from the wall surface of the pressure side, it will be described as "inrush" or "uplift," respectively. Based on the counter-rotation of these streamwise vortices and their mutual induction, the tip-aligned plane is subjected to an inrush of high momentum fluids, leading to a fuller velocity profile (see Fig. 11), lower level of TKE, and thinning of the wake shear layer. On the other hand, the root-aligned plane is besieged by the uplift of the low momentum fluids, which will initiate an inflectional instability process to produce a relatively high TKE free shear layer atop, and co-exists with the wake shear layer. As reported earlier, the *H*45*L*45 serrated leading edge will cause a broadband noise increase in frequency *zone* 4. The turbulent shear layer is expected to be only a relatively weak quadrupole noise source, which by itself is not capable of causing a broadband noise increase in frequency *zone* 4. Rather, the small vertical displacement between the turbulent shear layer created by the streamwise vortical structures and the trailing edge would facilitate an instantaneous transition to a predominantly dipole edge noise radiation mechanism. This phenomenon has been reported elsewhere by the co-authors (Lacagnina *et al.*, 2019) of this paper, albeit in the context of trailing edge noise radiation at the near-stall condition. We found that the instability in the separated shear layer can produce strong hydrodynamic pressure fluctuations close to the trailing edge, which then scatter into sound. The broadband noise increase in frequency *zone* 4 by the *H*45*L*45 serrated aerofoil in the current case is, therefore, related to the high TKE free shear layer generated at the

root-aligned plane of the pressure side through a similar mechanism as the one described by Lacagnina *et al.* (2019), which, in essence, is the turbulent–trailing edge broadband noise radiated from the pressure side of the aerofoil.

Despite sharing the same serration amplitude, one might question the lack of broadband noise increase in frequency *zone* 4 for the *H*45*L*7.5 serrated leading edge at $U_\infty = 20$ m/s. The reason is due to the much smaller serration wavelength of the *H*45*L*7.5, where the streamwise vortices would have already been coalesced before reaching the trailing edge. Therefore, there is no mechanism to uplift the low momentum fluid to generate the free shear layer as the extraneous noise source. Nevertheless, the broadband noise increase is shown to happen when $U_\infty = 60$ m/s for the *H*45*L*7.5 (Fig. 10). This might be due to the delay in coalescence of the streamwise vortices at such high inflow velocity so that a similar mechanism depicted in Fig. 12 will happen. This remains to be verified in future tests. The large serration wavelength is prone to produce an additional free shear layer through the inflectional instability. Despite the fact that the *H*7.5*L*45 serrated aerofoil also possesses similar inflectional profiles at the root-aligned plane (results are not shown here for brevity), its small serration amplitude does not enable the turbulent shear layer to become an effective hydrodynamic disturbance to the trailing edge because of the weaker streamwise vortices generated.

V. CONCLUSION

Initially, two trailing edge noise sources have been identified to contribute in the far field radiation by an asymmetric aerofoil with a blunt trailing edge. The first is related to the bluntness-induced coherent and spanwise structures in the wake region where the velocity fluctuations caused by the shedding cycle would resonate to the far field in the form of narrowband radiation. The second noise source is related to the boundary layer instability scattering at the blunt edge (suction side only). These two noise sources coexist in the acoustic spectra but occur at different frequencies, resulting in the appearance of double tonal radiation. The paper demonstrates that the use of the serrated leading edge can manipulate the two trailing edge noise sources considerably.

With regard to the bluntness-induced tonal noise radiation, the central control strategy is to disrupt the growth of the spanwise coherent structures in the wake. Results show that a combination of the large serration amplitude and small serration wavelength at the leading edge can inject streamwise vorticity beyond the trailing edge and into the wake, suppressing the coherent eigenmodes and tonal noise radiation. This control mechanism would be ineffective when the serrated leading edge is of a small serration amplitude and/or large serration wavelength due to the weaker streamwise vortices generated and compartmentalisation of the wake vortex shedding, respectively.

With regard to the boundary layer instability tonal noise radiation, the control strategy is to suppress the separation bubble near the trailing edge. A large serration amplitude at the leading edge is not very essential because the generated streamwise vortices only need to sustain into the vicinity of the trailing edge. The most effective leading edge geometry would be those with a small serration wavelength as this entails a large number of spanwise arrays of streamwise vortices generated to facilitate a greater level of destructive interaction with the separation region downstream.

Interestingly, implementing a serrated leading edge with both large serration amplitude and wavelength can create a third trailing edge noise source that is well reflected in the acoustic spectra. Essentially, strong counter-rotating streamwise vortices that are adequately spaced in the spanwise direction at the aerofoil's pressure side can mutually induce against each other. One consequence of such induction is the uplift of low momentum fluids to cause an inflectional velocity profile at the outer layer. The instability, after undergoing what is possibly an inviscid Kelvin-Helmholtz mechanism, would grow as a turbulent shear layer. The turbulent shear layer, though by itself it is not expected to be an effective noise source, will produce strong hydrodynamic pressure fluctuations to the trailing edge, which then scatter into broadband noise and transform into a trailing edge noise mechanism. We should emphasise that such a dynamic of fluids is highly dependent on the serration geometry, aerofoil type, Reynolds number, and angle of attack (i.e., pressure gradient effect).

As a concluding remark, the serrated leading edge can be an effective device to manipulate the flow field at the trailing edge (blunt or sharp) even when the boundary layer at the trailing edge is fully turbulent. After the injection of counter-rotating streamwise structures to the trailing edge, it has been shown in Fig. 17 of Chong *et al.* (2018) that the inrush of high momentum fluids toward the wall can relaminarise the boundary layer. The uplift of low momentum fluid, in the absence of a preexisting inflectional mechanism in a turbulent boundary layer, can instead push the turbulent source away from the wall. Both manipulations could reduce the efficiency of turbulent broadband noise scattering at the trailing edge. Further details about this topic will be discussed elsewhere.

ACKNOWLEDGMENTS

This work is supported by the UK Engineering and Physical Sciences Research Council research grant (Grant No. EP/N018737/1) "Quiet aerofoils of the next-generation."

Al-Sadawi, L., Chong, T. P., and Kim, J. H. (**2019**). "Aerodynamic noise reduction by plasma actuators for a flat plate with blunt trailing edge," J. Sound Vib. **439**, 173–193.

Berkooz, G., Holmes, P., and Lumley, J. L. (**1993**). "The proper orthogonal decomposition in the analysis of turbulent flows," Annu. Rev. Fluid Mech. **25**, 539–575.

Biedermann, T. M., Chong, T. P., Kameier, F., and Paschereit, C. O. (**2017**). "Statistical-empirical modelling of airfoil noise subjected to leading edge serrations," AIAA J. **55**, 3128–3142.

Blake, W. K. (**1986**). *Mechanics of Flow-Induced Sound and Vibration, Volume II: Complex Flow-Structure Interaction* (Academic Press, London).
Brooks, T. F., and Schlinker, R. (**1983**). "Progress in rotor broadband noise research," Vertica **7**, 287–307.
Brooks, T. F., Pope, S., and Marcolini, M. A. (**1989**). "Airfoil self-noise and prediction," NASA Reference Publication–1218 (NASA, Langley, VA).
Chaitanya, P., Joseph, P. F., Narayanan, S., and Vanderwel, C. (**2017**). "Performance and mechanism of sinusoidal leading edge serrations for the reduction of turbulence–aerofoil interaction noise," J. Fluid Mech. **818**, 435–464.
Chong, T. P., Biedermann, T., Koster, O., and Hasheminejad, S. M. (**2018**). "On the effect of leading edge serrations on aerofoil noise production," in *24th AIAA/CEAS Aeroacoustic Conference and Exhibit*, AIAA Paper No. 2018-3289, Atlanta, Georgia.
Chong, T. P., and Joseph, P. F. (**2012**). "'Ladder' structure in tonal noise generated by laminar flow around an airfoil," J. Acoust. Soc. Am. **131**, EL461–EL467.
Chong, T. P., and Joseph, P. F. (**2009**). "An experimental study of tonal noise mechanism of laminar airfoils," in *15th AIAA/CEAS Aeroacoustic Conference and Exhibit*, AIAA Paper No. 2009-3345, Miami, FL.
Fish, F. E., Weber, P. W., Murray, M. M., and Howle, L. E. (**2011**). "The tubercles on humpback whales' flippers: Application of bio-inspired technology," Integr. Comp. Biol. **51**, 203–213.
Hansen, K. L., Kelso, R. M., and Dally, B. B. (**2011**). "Performance variations of leading edge tubercles for distinct airfoil profiles," AIAA J. **49**, 185–194.
Johari, H., Henoch, C. W., Custodio, D., and Levshin, A. (**2007**). "Effects of leading-edge protuberances on airfoil performance," AIAA J. **45**, 2634–2642.
Kim, J. W., Haeri, S., and Joseph, P. F. (**2016**). "On the reduction of aerofoil–turbulence interaction noise associated with wavy leading edges," J. Fluid Mech. **792**, 526–552.
Lacagnina, G., Chaitanya, P., Berk, T., Kim, J. H., Joseph, P. F., Ganapathisubramani, B., Hasheminejad, S. M., Chong, T. P., Stalnov, O., Choi, K. S., Shahab, M. F., Omidyeganeh, M., and Pinelli, A. (**2019**). "Investigation of the aerofoil noise near stall conditions," Phys. Rev. Fluids **4**, 123902.
Lin, J. C. (**2002**). "Review of research on low-profile vortex generators to control boundary-layer separation," Prog. Aerosp. Sci. **38**, 389–420.
Miklosovic, D. S., Murray, M. M., Howle, L. E., and Fish, F. E. (**2004**). "Leading edge tubercles delay stall on a humpback whale flipper," Phys. Fluids **16**, L39–L42.
Nash, E. C., Lowson, M. V., and McAlpine, A. (**1999**). "Boundary layer instability noise on airfoils," J. Fluid Mech. **382**, 27–61.
Roshko, A. (**1995**). "On the wake and drag of bluff bodies," J. Aeronaut. Sci. **22**, 124–132.
Rostamzadeh, N., Kelso, R. M., Dally, B. B., and Tian, Z. F. (**2012**). "An experimental and computational study of flow over a NACA 0021 airfoil with wavy leading edge modification," in *18th Australasian Fluid Mechanics Conference*, Launceston, Australia.
Showkat Ali, S. A., Azarpeyvand, M., and Ilario da Silva, C. R. (**2018**). "Trailing-edge flow and noise control using porous treatments," J. Fluid Mech. **850**, 83–119.
Skillen, A., Revell, A., Pinelli, A., Piomelli, U., and Favier, J. (**2015**). "Flow over a wing with leading-edge undulations," AIAA J. **53**, 464–472.
Standish, K., and Van Dam, C. (**2003**). "Aerodynamic analysis of blunt trailing edge airfoils," Trans. ASME: J. Sol. Energy Eng. **125**, 479–487.
Van Nierop, E. A., Alben, S., and Brenner, M. P. (**2008**). "How bumps on whale flippers delay stall: An aerodynamic model," Phys. Rev. Lett. **100**, 054502.
Vathylakis, A., Chong, T. P., and Kim, J. H. (**2014**). "Design of a low-noise aeroacoustic wind tunnel facility at Brunel University," in *20th AIAA/CEAS Aeroacoustic Conference and Exhibit*, AIAA Paper No. 2014-3288, Atlanta, Georgia.
Winnemöller, T., and Dam, C. P. V. (**2007**). "Design and numerical optimization of thick airfoils including blunt trailing edges," J. Aircr. **44**, 232–240.